Science Advances
AAAS

Supplementary Materials for

Global oceanic oxygenation controlled by the Southern Ocean through the last deglaciation

Yi Wang *et al.*

Corresponding author: Yi Wang, ywang@whoi.edu, ywang145@tulane.edu

Sci. Adv. **10**, eadk2506 (2024)
DOI: 10.1126/sciadv.adk2506

The PDF file includes:

Other Supplementary Material for this manuscript includes the following:

Supplementary Text

Compilation of paleo-oxygenation reconstructions

Bottom water oxygenation reconstructions shown in the Figure 2 were drawn from previous compilations (*2*, *3*, *74*), with the addition of recently published data (*1*, *14*, *75–91*) (Table S1). A total of 229 records were included, covering a water depth range of 120 – 7118 m. The local redox proxies used in the reconstructions included sedimentary laminations (preserved under oxygen deficiency due to the lack of bioturbation by macrofauna) (*92*), foraminiferal assemblages (*93*, *94*), bulk sedimentary $\delta^{15}N$ (*95*), redox-sensitive trace metals (e.g., Mn, U, Re, and Mo) (*96*), alkenone concentrations (*97*), foraminiferal $\delta^{13}C$ (*17*) and I/Ca (*98*), and the foraminiferal porosity (*99*). Different proxies have different sensitivities to bottom water oxygen and result in records providing both qualitative (e.g., lamination) and various degrees of quantitative oceanic oxygenation reconstructions. Oxygenation changes between the Last Glacial Maximum (LGM, 19-23 kyr BP) and the Holocene (0-11.7 kyr BP) were determined from the original publications based on the proxy records generated. When multiple proxies were measured on the same core that yielded different interpretations, the oxygenation difference was determined as 'ambiguous'. The age models in the original publications were not modified. Age uncertainties are less of an issue when comparing the LGM and Holocene changes, as the two climate states can be distinguished from oxygen isotope stratigraphy and are usually accompanied by significant oxygen difference.

Ocean volume and seafloor area determination

The ocean volume and seafloor area below and above 1500 m was calculated using the ETOPO1 (10.7289/V5C8276M), a 1 arc-minute global relief model derived by NOAA National Geophysical Data Center. The global relief model was first remapped onto the cylindrical equal area projection in ArcGIS. The ocean volume and seafloor area by depth was then calculated using the 'Surface Volume' tool. The ocean volume below 1500 m water depth was determined to be 0.846×10^9 km^3, or 63.3% of the total ocean volume; whereas the seafloor area below 1500 m was 3.12×10^8 km^2 (84.7% of the total seafloor area).

Modern Tl mass balance model

A single one-box model that tracks sources and sinks of seawater Tl can be written as:

$$\frac{dN_{sw}}{dt} = F_{in} - F_{out} = \left(F_{river} + F_{hydrothermal} + F_{aerosol} + F_{volcanic}\right) - \left(F_{oxic} + F_{crust} + F_{low-oxygen}\right) \quad (1)$$

where N_{sw} denotes the amount of Tl in the ocean reservoir. F_{in} and F_{out} are input (source) and output (sink) fluxes, respectively (see Table S3 for a summary). Riverine, hydrothermal, dust aerosol, and volcanic emissions input fluxes are respectively denoted by F_{river}, $F_{hydrothermal}$, $F_{aerosol}$, and $F_{volcanic}$ (*6*, *100*). The main output fluxes include Mn oxide burial (F_{oxic}) and alteration of oceanic crust F_{crust}. Another minor sink ($F_{low\text{-}oxygen}$) usually occurs in low-oxygen environments, with quantitative Tl removal at/near the sediment-water interface due to reducing porewaters and thus no net Tl isotope fractionation from the overlying water column (*10*, *11*). This flux has recently been estimated using modern sediment core tops on the continental margin at 0.40×10^6 mol/yr (*11*). The isotopic mass balance takes the form as

$$\frac{d\varepsilon^{205}Tl_{sw}}{dt} = \frac{\sum\left[F_{in}\left(\varepsilon^{205}Tl_{in} - \varepsilon^{205}Tl_{sw}\right)\right] - \sum\left[F_{in}\left(\varepsilon^{205}Tl_{out} - \varepsilon^{205}Tl_{sw}\right)\right]}{N_{sw}} \quad (2)$$

where $\varepsilon^{205}Tl_{in}$, $\varepsilon^{205}Tl_{out}$, and $\varepsilon^{205}Tl_{sw}$ represent Tl isotopic compositions of inputs, outputs, and seawater, respectively. As the isotopic compositions of the input fluxes are all around -2, seawater $\varepsilon^{205}Tl$ is modulated by oceanic Tl sinks (*6*). Although Tl input fluxes may be variable, an increase in the input fluxes would need to be balanced by increasing output fluxes (either the oceanic crust alteration and/or Mn oxide burial) to reach steady state. As both these sinks depend on the size of the seawater Tl reservoir, it is expected that increased inputs would equally affect the two major output fluxes, resulting in zero net Tl isotope change in seawater. As the oceanic crust alteration sink is relatively stable on timescales shorter than 1 million years (*6*), Mn oxides are the only likely vector of significant Tl isotope variation in seawater on such time scales. Thus, Mn oxide burial should be the primary driver of $\varepsilon^{205}Tl_{sw}$ perturbations over glacial timescales.

Manganese oxide precipitation is a function of the overall dissolved Mn(II) reservoir and dissolved oxygen in the water columns (*101*). Dissolved Mn(II) concentrations is affected by reductive dissolution of Mn oxides in the water columns and/or in sediment porewaters (*37*, *102*), supply from organic carbon remineralization (*101*), and/or lateral transport from the reducing shelf (*37*). For the steady-state calculation, Tl sink associated with the Mn oxide burial flux was perturbed and the marine Tl mass balance was given sufficient time to achieve the new equilibrium. The Holocene and the LGM steady state $\varepsilon^{205}Tl_{sw}$ values were set as -6 (modern seawater value) and -5.1 (average of the LGM in our record), respectively. If we assume that Tl scavenged by Mn oxides has a linear response to the Mn oxide burial (or Mn oxide precipitation rate) changes (e.g., 10% reduction of Mn oxide burial reduction corresponds to 10% reduction of Tl sink through this pathway), the steady state calculation would yield an 18% lower Mn oxide burial in the LGM relative to the Holocene. The long-term external reproducibility of Tl isotope measurements (0.3 $\varepsilon^{205}Tl$-units) was used to estimate the error on the calculated Mn oxide burial flux changes, which would result in a ~6% error bar. Although the deep ocean oxygen content is lower than present, we do not expect to see extreme reduction in Mn oxide burial fluxes during the LGM compared to the Holocene, because ample evidence has suggested that the majority of the ocean still had oxygen in LGM bottom waters (*17*). Lower oxygen content in the deep ocean could have enhanced Mn reductive dissolution in the porewaters that allows Mn(II) diffusion into the overlying bottom waters, and decreased the Mn oxide precipitation rates at the same time. Both processes would have kept increasing the dissolved Mn(II) reservoir in the ocean until a new equilibrium was reached, where the rates of Mn(II) oxidation and Mn oxide scavenging balanced the Mn(II) supply.

During the last deglaciation, millennial changes in $\varepsilon^{205}Tl_{sw}$ suggest non-steady-state variations that could have been caused by substantial short-term changes in Tl scavenging via Mn oxide precipitation variability. To simulate the transient changes of $\varepsilon^{205}Tl_{sw}$, the LOESS fit of authigenic $\varepsilon^{205}Tl$ was first interpolated evenly on 1000-year spacing (roughly the timescale of ocean mixing), which was also used as the time step in the Monte Carlo forward isotope mass balance modeling. The prior distribution of Mn oxide burial flux change was set as a uniform distribution varying between 0% and 500% of the modern steady state with 100000 realizations. Misfit of each realization was evaluated using the normalized L_2^2:

$$L_2^2 = \sum_{i=1}^{N} \frac{(\widehat{d_i} - d_i)^2}{\sigma_i^2} \qquad (3)$$

where $\widehat{d_i}$ is the model simulated value and d_i is the observation (LOESS fit of authigenic ε^{205}Tl). σ_i^2 is the standard deviation of observed authigenic ε^{205}Tl values. The likelihood (L) of each prediction is calculated by the Gaussian distribution ($L = e^{-\frac{L_2^2}{2}}$). Realizations with the top 5% of the likelihood were retained as the posterior distribution shown in Fig. S5.

Because of rapid Mn cycling in the global ocean, significant Mn oxide burial flux changes are likely to occur on short timescales in response to ambient oxygen variations (*15*, *103*, *104*), which would then trigger transient $\varepsilon^{205}Tl_{sw}$ changes on millennial timescales that can be recorded in the sedimentary archives (Fig. S5). Re-oxygenation of the deep ocean during HS1 (from the authigenic Tl isotope record) following the LGM would have increased Mn oxide precipitation rates, leading to a pulse of Mn oxide burial that exceeded the modern mass balance owing to the larger Mn(II) reservoir during the LGM. An abrupt transition from HS1 into B-A/ACR was accompanied by AMOC resumption (*42*) and re-stratification of the Southern Ocean (*27*), which could have triggered reductive dissolution of Mn oxides and Mn(II) supply from organic carbon remineralization. It is likely that reorganization of ocean circulation and deep ocean oxygenation effectively facilitated reduction of excessive Mn oxide burial during HS1 and reduced the Mn oxide precipitation rates, resulting in short-term decline of Mn oxide burial fluxes and a high Mn(II) reservoir in B-A/ACR. Additionally, oxygen minimum zone (OMZ) expansion and intensification in the upper North Pacific during B-A (*78*, *105*, *106*) could also have increased the deep ocean Mn(II) reservoir via lateral transport from the reducing OMZ sediments. Following the B-A/ACR with elevated Mn(II), a similar mechanism to HS1 that includes excess Mn oxide burial due to deep ocean reoxygenation can be used to explain the short-term Mn oxide burial changes in the YD.

It is also noted that manganese oxide precipitation rates could also be affected by Mn(II) concentrations in the water column (*107*), and hydrothermal Mn input may thus change Mn oxide precipitation rates in addition to dissolved oxygen control. Elevated hydrothermal Mn fluxes have been implied during the last deglaciation (peak at ~12-15 kyr BP), which was attributed to a lagged response to the sea level fall during the LGM (*108*). However, the maximum hydrothermal Mn influxes coincide with the low-oxygen interval during the B-A/ACR based on the ε^{205}Tl record, suggesting that hydrothermal Mn input should not have controlled the Mn oxide burial. Furthermore, Mn oxides precipitated proximally of hydrothermal vents are often dominated by todorokite (*109*), which does not exhibit strong Tl enrichments or any Tl isotope fractionation via oxidative sorption (*8*, *9*).

The observed millennial changes are unlikely to be a local/basin-only signal. None of the local oxygenation proxies, including redox-sensitive trace metals, foraminiferal I/Ca, and benthic foraminiferal porosity (*14*), show significant changes in the bottom water oxygenation/oxygen minimum zone intensity until the Holocene (Fig. S1), contradicting with control of local Mn oxide burial flux changes on $\varepsilon^{205}Tl_{sw}$ through the deglaciation. Additionally, NADW export to the deep Indian Ocean has been shown to increase during the deglaciation, especially after the B-A/ACR as AMOC resumed (*41*, *110*, *111*). A better communication between the Indian Ocean and NADW during the deglaciation would then argue against the interpretation that the authigenic ε^{205}Tl record only represents Indian Ocean basin changes.

We also caution that there is no quantitative conversion from Tl burial flux scavenged by Mn oxides to global oceanic oxygen concentration changes. We thus only limit our discussion on the qualitative oceanic DO content variability (i.e., direction of the change) indicated by the seawater ε^{205}Tl reconstruction. More detailed research is still required to better understand the timescales and magnitudes of Mn oxide burial flux variations in response to oceanic oxygenation and the underlying mechanisms.

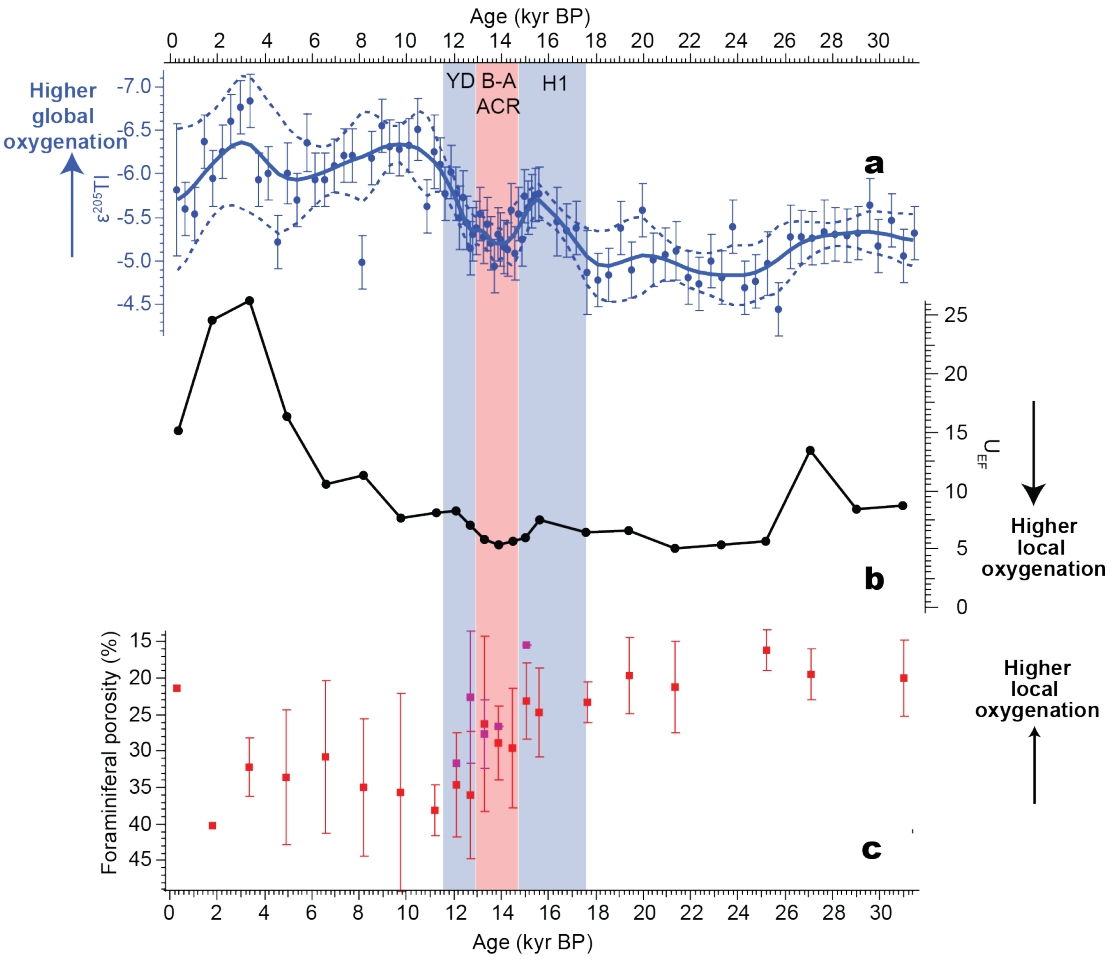

Fig. S1.

Authigenic ε^{205}Tl and bulk metal enrichment factors downcore. (a) Authigenic ε^{205}Tl with the LOESS fit (solid blue) and 2SD (dashed blue) from Fig. 2; (b) U enrichment factors with respect to ref. (*70*). The enrichment factor data were used in the decision tree (*11*) to determine the fidelity of the sediment archive in recording the seawater value. (c) Benthic foraminiferal porosity that shows local bottom water oxygenation changes from the core TN041-8PG/JPC (*14*). The decoupled responses of authigenic Tl isotope records and local oxygenation changes in the Arabian Sea oxygen minimum zone suggest that authigenic ε^{205}Tl is not affected by local controlling mechanisms (e.g., ventilation and productivity).

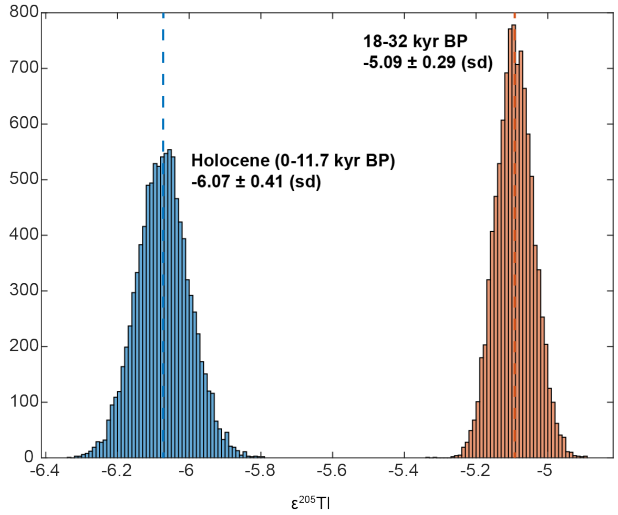

Fig. S2.
Bootstrapped sample distributions of Holocene and 18-32 kyr BP.

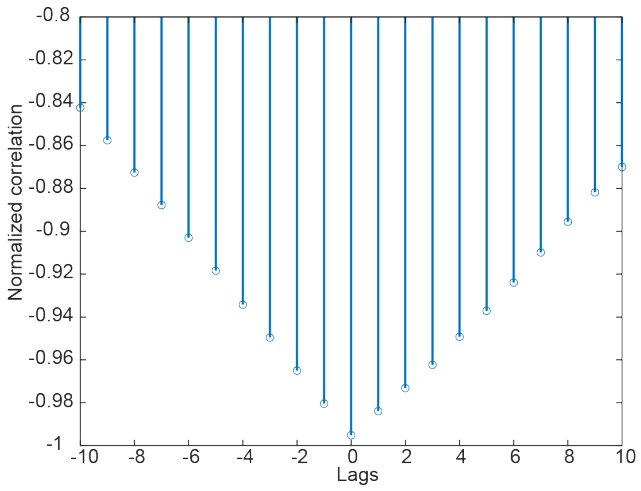

Fig. S3.

Normalized cross correlation between atmospheric pCO_2 (*52*) and authigenic Tl isotopic compositions, which shows the highest correlation when no time lag is applied.

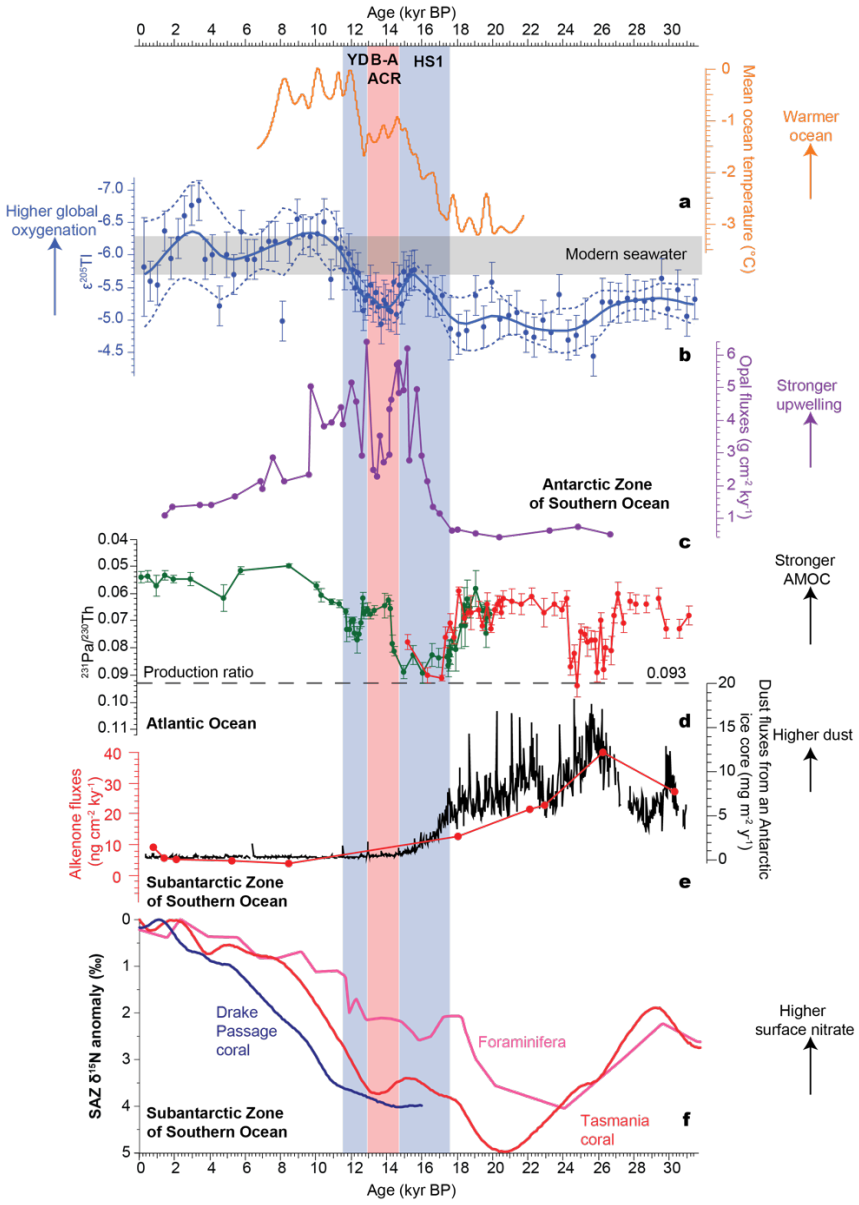

Fig. S4.

Authigenic ε^{205}Tl comparison with export productivity and temperature records. (a) Reconstructed mean ocean temperature from ice core (*22*). (b)-(d) were from Fig. 2. (b) authigenic sedimentary ε^{205}Tl record with the LOESS fit (solid blue) and 2SD (dashed blue); (c) Opal fluxes in the Southern Ocean (*27*); (d) ^{231}Pa/^{230}Th from the Bermuda Rise (*42*, *43*) with the production ratio in the water columns shown in the horizontal dashed line. (e) Dust fluxes from the EPICA Dome C ice core (black curve) (*112*) and alkenone fluxes from the core TN057-6/ODP 1090 (*23*) (red curve). (f) comparison of the Subantarctic Zone coral-bound mean δ^{15}N records (*39*) (blue and red curve) with the ODP Site 1090 foraminifera-bound δ^{15}N record in pink (*23*). The reduced export productivity and elevated (and relatively stable) surface nutrient levels suggest that the Subantarctic Zone contributed less to the deep ocean export carbon, and thus may not be the primary driver of the observed deglacial global DO changes.

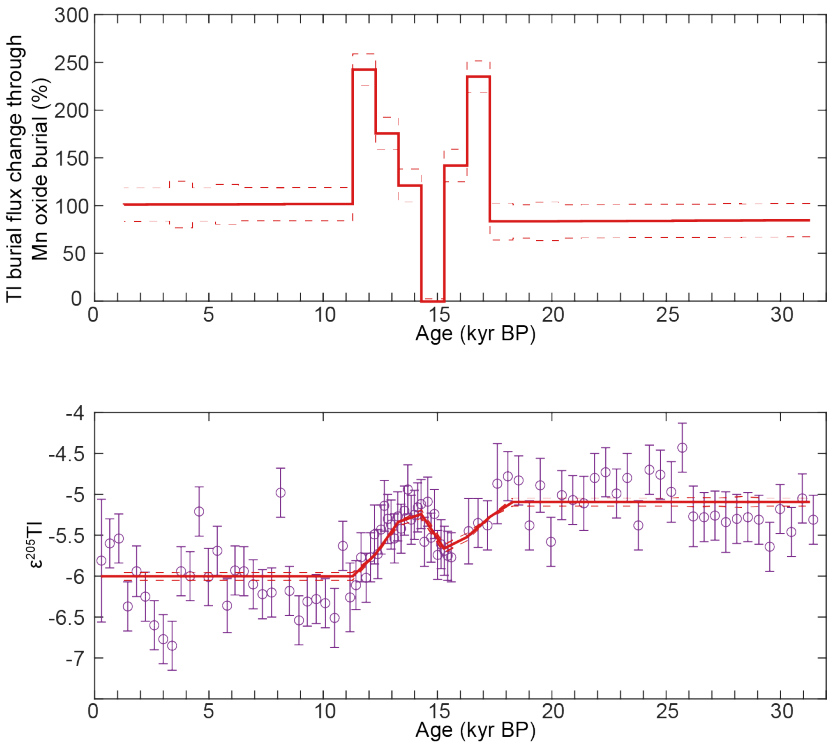

Fig. S5.

Forward transient (non-steady-state) mass balance model results starting from the LGM steady state (32 kyr BP) to present. Upper panel: Best fit (red solid) with the upper and lower limit (red dashed) of accepted Tl burial flux changes associated with Mn oxide burial. Lower panel: Observed authigenic Tl isotopic compositions (purple circles) with the modeled values (solid red as the best fit with the dashed red as the accepted envelope).

Table S1. (separate file)

Compilation of localized oceanic oxygenation reconstructions.

Table S2. (separate file)

Bulk elemental concentrations and authigenic Tl isotopic compositions.

Sources /Sinks	**Best estimate: modern (10^6 mol/yr)**	**ε^{205}Tl**	**References**
Rivers	1.13	-2.5	(*114*, *115*)
Hydrothermal fluids	0.83	-2.0	(*116*)
Subaerial volcanism	1.81	-2.1	(*7*, *115*, *117*)
Mineral aerosols	0.25	-2.0	(*115*)
Total input flux	4.02	-2.2	
Pelagic clays	1.52	10.0	(*7*, *115*)
Altered oceanic crust	2.10	-10.3	This study
Low-oxygen sediments with no net Tl fractionation	0.40	-6.0	(*12*)
Total output flux	4.02	-2.2	
	Total		**Steady-state residence time (ky)**
Global oceans	88000	-6.0	21.9

Table S3.

Updated modern Tl mass balance.

REFERENCES AND NOTES

1. S. L. Jaccard, E. D. Galbraith, A. Martínez-Garciá, R. F. Anderson, Covariation of deep Southern Ocean oxygenation and atmospheric CO_2 through the last ice age. *Nature* **530**, 207–210 (2016).

2. S. L. Jaccard, E. D. Galbraith, Large climate-driven changes of oceanic oxygen concentrations during the last deglaciation. *Nat. Geosci.* **5**, 151–156 (2012).

3. A. W. Jacobel, R. F. Anderson, S. L. Jaccard, J. F. McManus, F. J. Pavia, G. Winckler, Deep Pacific storage of respired carbon during the last ice age: Perspectives from bottom water oxygen reconstructions. *Quat. Sci. Rev.* **230**, 106065 (2020).

4. Y. Zhou, J. F. McManus, Authigenic uranium deposition in the glacial North Atlantic: Implications for changes in oxygenation, carbon storage, and deep water-mass geometry. *Quat. Sci. Rev.* **300**, 107914 (2023).

5. C. Deutsch, H. Brix, T. Ito, H. Frenzel, L. A. Thompson, Climate-forced variability of ocean hypoxia. *Science* **333**, 336–339 (2011).

6. E. D. Galbraith, S. L. Jaccard, Deglacial weakening of the oceanic soft tissue pump: Global constraints from sedimentary nitrogen isotopes and oxygenation proxies. *Quat. Sci. Rev.* **109**, 38–48 (2015).

7. S. G. Nielsen, M. Rehkämper, J. Prytulak, Investigation and application of thallium isotope fractionation. *Rev. Mineral. Geochem.* **82**, 759–798 (2017).

8. Y. Wang, S. Bodin, J. S. Blusztajn, C. Ullmann, S. G. Nielsen, Orbitally paced global oceanic deoxygenation decoupled from volcanic CO2 emission during the middle Cretaceous Oceanic Anoxic Event 1b (Aptian-Albian transition). *Geology*, **50**, 1324–1328 (2022).

9. S. G. Nielsen, L. E. Wasylenki, M. Rehkämper, C. L. Peacock, Z. Xue, E. M. Moon, Towards an understanding of thallium isotope fractionation during adsorption to manganese oxides. *Geochim. Cosmochim. Acta* **117**, 252–265 (2013).

10. C. L. Peacock, E. M. Moon, Oxidative scavenging of thallium by birnessite: Explanation for thallium enrichment and stable isotope fractionation in marine ferromanganese precipitates. *Geochim. Cosmochim. Acta* **84**, 297–313 (2012).

11. J. D. Owens, S. G. Nielsen, T. J. Horner, C. M. Ostrander, L. C. Peterson, Thallium-isotopic compositions of euxinic sediments as a proxy for global manganese-oxide burial. *Geochim. Cosmochim. Acta* **213**, 291–307 (2017).

12. Y. Wang, W. Lu, K. M. Costa, S. G. Nielsen, Beyond anoxia: Exploring sedimentary thallium isotopes in paleo-redox reconstructions from a new core top collection. *Geochim. Cosmochim. Acta* **333**, 347–361 (2022).

13. G. J. Reichart, S. J. Schenau, G. J. De Lange, W. J. Zachariasse, Synchroneity of oxygen minimum zone intensity on the Oman and Pakistan Margins at sub-Milankovitch time scales. *Mar. Geol.* **185**, 403–415 (2002).

14. S. J. A. Jung, D. Kroon, G. Ganssen, F. Peeters, R. Ganeshram, Enhanced Arabian Sea intermediate water flow during glacial North Atlantic cold phases. *Earth Planet. Sci. Lett.* **280**, 220–228 (2009).

15. W. Lu, Y. Wang, D. W. Oppo, S. G. Nielsen, K. M. Costa, Comparing paleo-oxygenation proxies (benthic foraminiferal surface porosity, I/Ca, authigenic uranium) on modern sediments and the glacial Arabian Sea. *Geochim. Cosmochim. Acta* **331**, 69–85 (2022).

16. A. Mangini, A. Eisenhauer, P. Walter, Response of manganese in the ocean to the climatic cycles in the Quaternary. *Paleoceanogr. Paleoclimatol.* **5**, 811–821 (1990).

17. E. D. Galbraith, M. Kienast, T. F. Pedersen, S. E. Calvert, Glacial-interglacial modulation of the marine nitrogen cycle by high-latitude O_2 supply to the global thermocline. *Paleoceanogr. Paleoclimatol.* **19**, 1–12 (2004).

18. B. A. A. Hoogakker, H. Elderfield, G. Schmiedl, I. N. McCave, R. E. M. Rickaby, Glacial–interglacial changes in bottom-water oxygen content on the Portuguese margin. *Nat. Geosci.* **8**, 40–43 (2015).

19. L. C. Skinner, E. Freeman, D. Hodell, C. Waelbroeck, N. Vazquez Riveiros, A. E. Scrivner, Atlantic ocean ventilation changes across the last deglaciation and their carbon cycle implications. *Paleoceanogr. Paleoclimatol.* **36**, e2020PA004074 (2021).

20. E. L. Sikes, C. R. Samson, T. P. Guilderson, W. R. Howard, Old radiocarbon ages in the southwest Pacific Ocean during the last glacial period and deglaciation. *Nature* **405**, 555–559 (2000).

21. L. Menviel, J. Yu, F. Joos, A. Mouchet, K. J. Meissner, M. H. England, Poorly ventilated deep ocean at the last glacial maximum inferred from carbon isotopes: A data-model comparison study. *Paleoceanography* **32**, 2–17 (2017).

22. E. Cliff, S. Khatiwala, A. Schmittner, Glacial deep ocean deoxygenation driven by biologically mediated air–sea disequilibrium. *Nat. Geosci.* **14**, 43–50 (2021).

23. B. Bereiter, S. Shackleton, D. Baggenstos, K. Kawamura, J. Severinghaus, Mean global ocean temperatures during the last glacial transition. *Nature* **553**, 39–44 (2018).

24. A. Martínez-García, D. M. Sigman, H. Ren, R. F. Anderson, M. Straub, D. A. Hodell, S. L. Jaccard, T. I. Eglinton, G. H. Haug, Iron fertilization of the subantarctic ocean during the last ice age. *Science* **343**, 1347–1350 (2014).

25. K. M. Costa, J. F. McManus, R. F. Anderson, H. Ren, D. M. Sigman, G. Winckler, M. Q. Fleisher, F. Marcantonio, A. C. Ravelo, No iron fertilization in the equatorial Pacific Ocean during the last ice age. *Nature* **529**, 519–522 (2016).

26. G. Winckler, R. F. Anderson, S. L. Jaccard, F. Marcantonio, Ocean dynamics, not dust, have controlled equatorial Pacific productivity over the past 500,000 years. *Proc. Natl. Acad. Sci. U. S. A.* **113**, 6119–6124 (2016).

27. S. L. Jaccard, E. D. Galbraith, D. M. Sigman, G. H. Haug, A pervasive link between Antarctic ice core and subarctic Pacific sediment records over the past 800kyrs. *Quat. Sci. Rev.* **29**, 206–212 (2010).

28. R. F. Anderson, S. Ali, L. I. Bradtmiller, S. H. H. Nielsen, M. Q. Fleisher, B. E. Anderson, L. H. Burckle, Wind-driven upwelling in the southern ocean and the deglacial rise in atmospheric CO_2. *Science* **323**, 1443–1448 (2009).

29. O. Cartapanis, D. Bianchi, S. L. Jaccard, E. D. Galbraith, Global pulses of organic carbon burial in deep-sea sediments during glacial maxima. *Nat. Commun.* **7**, 10796 (2016).

30. L. D. Stott, J. Shao, J. Yu, K. M. Harazin, Evaluating the glacial-deglacial carbon respiration and ventilation change hypothesis as a mechanism for changing atmospheric CO_2. *Geophys. Res. Lett.* **48**, e2020GL091296 (2021).

31. G. Gebbie, How much did Glacial North Atlantic Water shoal? *Paleoceanography* **29**, 190–209 (2014).

32. D. W. Oppo, G. Gebbie, K. F. Huang, W. B. Curry, T. M. Marchitto, K. R. Pietro, Data constraints on glacial atlantic water mass geometry and properties. *Paleoceanogr. Paleoclimatol.* **33**, 1013–1034 (2018).

33. L. C. Skinner, S. Fallon, C. Waelbroeck, E. Michel, S. Barker, Ventilation of the deep southern ocean and deglacial CO_2 rise. *Science* **328**, 1147–1151 (2010).

34. B. B. Stephens, R. F. Keeling, The influence of antarctic sea ice on glacial-interglacial CO_2 variations. *Nature* **404**, 171–174 (2000).

35. K. Matsumoto, T. Hashioka, Y. Yamanaka, Effect of temperature-dependent organic carbon decay on atmospheric pCO_2. *J. Geophys. Res. Biogeosci.* **112**, G02007 (2007).

36. R. Roth, S. P. Ritz, F. Joos, Burial-nutrient feedbacks amplify the sensitivity of atmospheric carbon dioxide to changes in organic matter remineralisation. *Earth Syst. Dyn.* **5**, 321–343 (2014).

37. L. Menviel, F. Joos, S. P. Ritz, Simulating atmospheric CO_2, ^{13}C and the marine carbon cycle during the Last Glacial-Interglacial cycle: Possible role for a deepening of the mean

remineralization depth and an increase in the oceanic nutrient inventory. *Quat. Sci. Rev.* **56**, 46–68 (2012).

38. G. P. Klinkhammer, M. L. Bender, The distribution of manganese in the Pacific Ocean. *Earth Planet. Sci. Lett.* **46**, 361–384 (1980).

39. G. Gebbie, P. Huybers, Total matrix intercomparison: A method for determining the geometry of water-mass pathways. *J. Phys. Oceanogr.* **40**, 1710–1728 (2010).

40. X. T. Wang, D. M. Sigman, M. G. Prokopenko, J. F. Adkins, L. F. Robinson, S. K. Hines, J. Chai, A. S. Studer, A. Martínez-García, T. Chen, G. H. Haug, Deep-sea coral evidence for lower Southern Ocean surface nitrate concentrations during the last ice age. *Proc. Natl. Acad. Sci. U. S. A.* **114**, 3352–3357 (2017).

41. L. C. Skinner, A. E. Scrivner, D. Vance, S. Barker, S. Fallon, C. Waelbroeck, North atlantic versus southern ocean contributions to a deglacial surge in deep ocean ventilation. *Geology* **41**, 667–670 (2013).

42. N. Bharti, R. Bhushan, L. Skinner, M. Muruganantham, P. S. Jena, A. Dabhi, A. Shivam, Evidence of poorly ventilated deep Central Indian Ocean during the last glaciation. *Earth Planet. Sci. Lett.* **582**, 117438 (2022).

43. J. F. McManus, R. Francois, J.-M. Gherardi, L. D. Keigwin, S. Brown-Leger, Collapse and rapid resumption of Atlantic meridional circulation linked to deglacial climate changes. *Nature* **428**, 834–837 (2004).

44. J. Lippold, J. Grützner, D. Winter, Y. Lahaye, A. Mangini, M. Christi, Does sedimentary $^{231}Pa/^{230}Th$ from the Bermuda rise monitor past Atlantic meridional overturning circulation? *Geophys. Res. Lett.* **36**, L12601 (2009).

45. H. C. Ng, L. F. Robinson, J. F. McManus, K. J. Mohamed, A. W. Jacobel, R. F. Ivanovic, L. J. Gregoire, T. Chen, Coherent deglacial changes in western Atlantic ocean circulation. *Nat. Commun.* **9**, 2947 (2018).

46. F. Pöppelmeier, A. Jeltsch-Thömmes, J. Lippold, F. Joos, T. F. Stocker, Multi-proxy constraints on Atlantic circulation dynamics since the last ice age. *Nat. Geosci.* **16**, 349–356 (2023).

47. Y. Dai, J. Yu, P. A. Rafter, Deglacial ventilation changes in the deep southwest pacific. *Paleoceanogr. Paleoclimatol.* **36**, e2020PA004172 (2021).

48. D. M. Sigman, F. Fripiat, A. S. Studer, P. C. Kemeny, A. Martínez-García, M. P. Hain, X. Ai, X. Wang, H. Ren, G. H. Haug, The Southern Ocean during the ice ages: A review of the Antarctic surface isolation hypothesis, with comparison to the North Pacific. *Quat. Sci. Rev.* **254**, 106732 (2021).

49. G. H. Denton, R. F. Anderson, J. R. Toggweiler, R. L. Edwards, J. M. Schaefer, A. E. Putnam, The last glacial termination. *Science* **328**, 1652–1656 (2010).

50. J. R. Toggweiler, J. L. Russell, S. R. Carson, Midlatitude westerlies, atmospheric CO_2, and climate change during the ice ages. *Paleoceanography* **21**, PA2005 (2006).

51. A. M. C. Hogg, M. P. Meredith, J. R. Blundel, C. Wilson, Eddy heat flux in the Southern ocean: Response to variable wind forcing. *J. Clim.* **21**, 608–620 (2008).

52. R. Ferrari, M. F. Jansen, J. F. Adkins, A. Burke, A. L. Stewart, A. F. Thompson, Antarctic sea ice control on ocean circulation in present and glacial climates. *Proc. Natl. Acad. Sci. U. S. A.* **111**, 8753–8758 (2014).

53. A. Schmittner, E. D. Galbraith, Glacial greenhouse-gas fluctuations controlled by ocean circulation changes. *Nature* **456**, 373–376 (2008).

54. B. Bereiter, S. Eggleston, J. Schmitt, C. Nehrbass-Ahles, T. F. Stocker, H. Fischer, S. Kipfstuhl, J. Chappellaz, Revision of the EPICA Dome C CO_2 record from 800 to 600 kyr before present. *Geophys. Res. Lett.* **42**, 542–549 (2015).

55. L. Menviel, P. Spence, J. Yu, M. A. Chamberlain, R. J. Matear, K. J. Meissner, M. H. England, Southern Hemisphere westerlies as a driver of the early deglacial atmospheric CO_2 rise. *Nat. Commun.* **9**, 2503 (2018).

56. J. Yu, L. Menviel, Z. D. Jin, D. J. R. Thornalley, G. L. Foster, E. J. Rohling, I. N. McCave, J. F. McManus, Y. Dai, H. Ren, F. He, F. Zhang, P. J. Chen, A. P. Roberts, More efficient North Atlantic carbon pump during the Last Glacial Maximum. *Nat. Commun.* **10**, 2170 (2019).

57. I. Marinov, A. Gnanadesikan, J. L. Sarmiento, J. R. Toggweiler, M. Follows, B. K. Mignone, Impact of oceanic circulation on biological carbon storage in the ocean and atmospheric pCO_2. *Global Biogeochem. Cycles* **22**, GB3007 (2008).

58. T. Chen, L. F. Robinson, A. Burke, J. Southon, P. Spooner, P. J. Morris, H. C. Ng, Synchronous centennial abrupt events in the ocean and atmosphere during the last deglaciation. *Science* **349**, 1537–1541 (2015).

59. R. Goyal, A. Sen Gupta, M. Jucker, M. H. England, Historical and projected changes in the Southern hemisphere surface Westerlies. *Geophys. Res. Lett.* **48**, e2020GL090849 (2021).

60. K. L. Gunn, S. R. Rintoul, M. H. England, M. M. Bowen, Recent reduced abyssal overturning and ventilation in the Australian Antarctic Basin. *Nat. Clim. Chang.* **13**, 537–544 (2023).

61. T. L. Frölicher, M. T. Aschwanden, N. Gruber, S. L. Jaccard, J. P. Dunne, D. Paynter, Contrasting upper and deep ocean oxygen response to protracted global warming. *Global Biogeochem. Cycles* **34**, e2020GB006601 (2020).

62. Y. You, Intermediate water circulation and ventilation of the Indian Ocean derived from water-mass contributions. *J. Mar. Res.* **56**, 1029–1067 (1998).

63. V. V. S. S. Sarma, An evaluation of physical and biogeochemical processes regulating perennial suboxic conditions in the water column of the Arabian Sea. *Global Biogeochem. Cycles* **16**, 29–1–29–11 (2002).

64. T. J. Heaton, P. Köhler, M. Butzin, E. Bard, R. W. Reimer, W. E. N. Austin, C. Bronk Ramsey, P. M. Grootes, K. A. Hughen, B. Kromer, P. J. Reimer, J. Adkins, A. Burke, M. S. Cook, J. Olsen, L. C. Skinner, Marine 20—The marine radiocarbon age calibration curve (0–55,000 cal BP). *Radiocarbon* **62**, 779–820 (2020).

65. J. Southon, M. Kashgarian, M. Fontugne, B. Metivier, W. W.-S. Yim, Marine reservoir corrections for the Indian ocean and southeast Asia. *Radiocarbon* **44**, 167–180 (2002).

66. M. Blaauw, J. A. Christeny, Flexible paleoclimate age-depth models using an autoregressive gamma process. *Bayesian Anal.* **6**, 457–474 (2011).

67. C. M. Ostrander, J. D. Owens, S. G. Nielsen, Constraining the rate of oceanic deoxygenation leading up to a Cretaceous Oceanic Anoxic Event (OAE-2: ~94 Ma). *Sci. Adv.* **3**, e1701020 (2017).

68. S. G. Nielsen, M. Rehkämper, J. Baker, A. N. Halliday, The precise and accurate determination of thallium isotope compositions and concentrations for water samples by MC-ICPMS. *Chem. Geol.* **204**, 109–124 (2004).

69. M. Rehkämper, M. Frank, J. R. Hein, D. Porcelli, A. Halliday, J. Ingri, V. Liebetrau, Thallium isotope variations in seawater and hydrogenetic, diagenetic, and hydrothermal ferromanganese deposits. *Earth Planet. Sci. Lett.* **197**, 65–81 (2002).

70. Y. Shu, S. G. Nielsen, Z. Zeng, R. Shinjo, J. Blusztajn, X. Wang, S. Chen, Tracing subducted sediment inputs to the Ryukyu arc-Okinawa Trough system: Evidence from thallium isotopes. *Geochim. Cosmochim. Acta* **217**, 462–491 (2017).

71. J. Ahrens, M. Beck, P. Böning, J. Degenhardt, K. Pahnke, B. Schnetger, H. J. Brumsack, Thallium cycling in pore waters of intertidal beach sediments. *Geochim. Cosmochim. Acta* **306**, 321–339 (2021).

72. R. L. Rudnick, S. Gao, “Composition of the continental crust” in *Treatise on Geochemistry*, vol. 3, H. D. Holland, K. K. Turekian, Eds. (Pergamon, 2003), pp. 1–64.

73. S. G. Nielsen, M. Goff, S. P. Hesselbo, H. C. Jenkyns, D. E. LaRowe, C.-T. A. Lee, Thallium isotopes in early diagenetic pyrite – A paleoredox proxy? *Geochim. Cosmochim. Acta* **75**, 6690–6704 (2011).

74. R. E. Chandler, E. M. Scott, *Statistical Methods for Trend Detection and Analysis in the Environmental Sciences* (John Wiley & Sons, 2011).

75. R. Schlitzer, Ocean Data View (2018). https://odv.awi.de.

76. Z. Erdem, J. Schönfeld, A. E. Rathburn, M. E. Pérez, J. Cardich, N. Glock, Bottom-water deoxygenation at the Peruvian margin during the last deglaciation recorded by benthic foraminifera. *Biogeosciences.* **17**, 3165–3182 (2020).

77. F. Marcantonio, R. Hostak, J. E. Hertzberg, M. W. Schmidt, Deep equatorial Pacific ocean oxygenation and atmospheric CO_2 over the last ice age. *Sci. Rep.* **10**, 6606 (2020).

78. Z. Lu, B. A. A. Hoogakker, C.-D. Hillenbrand, X. Zhou, E. Thomas, K. M. Gutchess, W. Lu, L. Jones, R. E. M. Rickaby, Oxygen depletion recorded in upper waters of the glacial Southern Ocean. *Nat. Commun.*, **7**, 11146 (2016).

79. S. E. Moffitt, T. M. Hill, P. D. Roopnarine, J. P. Kennett, Response of seafloor ecosystems to abrupt global climate change. *Proc. Natl. Acad. Sci. U. S. A.* **112**, 4684–4689 (2015).

80. A. Durand, Z. Chase, T. L. Noble, H. Bostock, S. L. Jaccard, A. T. Townsend, N. L. Bindoff, H. Neil, G. Jacobsen, Reduced oxygenation at intermediate depths of the southwest Pacific during the last glacial maximum. *Earth Planet. Sci. Lett.* **491**, 48–57 (2018).

81. M. Luo, T. J. Algeo, H. Tong, J. Gieskes, L. Chen, X. Shi, D. Chen, More reducing bottom-water redox conditions during the last glacial maximum in the southern challenger deep (Mariana trench, western pacific) driven by enhanced productivity. *Deep Sea Res. Part II Top. Stud. Oceanogr. DEEP-SEA RES PT II* **155**, 70–82 (2018).

82. J. Zou, X. Shi, A. Zhu, S. Kandasamy, X. Gong, L. Lembke-Jene, M. te Chen, Y. Wu, S. Ge, Y. Liu, X. Xue, G. Lohmann, R. Tiedemann, Millennial-scale variations in sedimentary

oxygenation in the western subtropical North Pacific and its links to North Atlantic climate. *Clim. Past* **16**, 387–407 (2020).

83. E. Ovsepyan, E. Ivanova, M. Tetard, L. Max, R. Tiedemann, Intermediate- and deep-water oxygenation history in the subarctic north pacific during the last deglacial period. *Front. Earth Sci.* **9**, 718 (2021).

84. G. Li, H. Rashid, L. Zhong, X. Xu, W. Yan, Z. Chen, Changes in deep water oxygenation of the south China sea since the last glacial period. *Geophys. Res. Lett.* **45**, 9058–9066 (2018).

85. Sharon, C. S. Belanger, J. Du, A. Mix, Reconstructing paleo-oxygenation for the last 54,000 years in the gulf of Alaska using cross-validated benthic foraminiferal and geochemical records. *Paleoceanogr. Paleoclimatol.* **36**, e2020PA003986 (2021).

86. Y. Dou, S. Yang, C. Li, X. Shi, J. Liu, L. Bi, Deepwater redox changes in the southern Okinawa Trough since the last glacial maximum. *Prog. Oceanogr.* **135**, 77–90 (2015).

87. D. Gallego-Torres, O. E. Romero, F. Martínez-Ruiz, J. H. Kim, B. Donner, M. Ortega-Huertas, Rapid bottom-water circulation changes during the last glacial cycle in the coastal low-latitude NE Atlantic. *Quatern. Res.* **81**, 330–338 (2014).

88. M. Tetard, L. Licari, L. Beaufort, Oxygen history off Baja California over the last 80 kyr: A new foraminiferal-based record. *Paleoceanography* **32**, 246–264 (2017).

89. W. Lu, C. F. Barbosa, A. E. Rathburn, P. da M. Xavier, A. P. S. Cruz, E. Thomas, R. E. M. Rickaby, Y. G. Zhang, Z. Lu, Proxies for paleo-oxygenation: A downcore comparison between benthic foraminiferal surface porosity and I/Ca. *Palaeogeogr. Palaeoclimatol. Palaeoecol.* **579**, 110588 (2021).

90. M. Wagner, I. L. Hendy, Trace metal evidence for a poorly ventilated glacial Southern Ocean. *Quat Sci Rev* **170**, 109–120 (2017).

91. B. Gaye, A. Böll, J. Segschneider, N. Burdanowitz, K. C. Emeis, V. Ramaswamy, N. Lahajnar, A. Lückge, T. Rixen, Glacial-interglacial changes and Holocene variations in Arabian Sea denitrification. *Biogeosciences* **15**, 507–527 (2018).

92. J. Gottschalk, L. C. Skinner, J. Lippold, H. Vogel, N. Frank, S. L. Jaccard, C. Waelbroeck, Biological and physical controls in the Southern Ocean on past millennial-scale atmospheric CO_2 changes. *Nat. Commun.* **7**, 11539 (2016).

93. A. van Geen, Y. Zheng, J. M. Bernhard, K. G. Cannariato, J. Carriquiry, W. E. Dean, B. W. Eakins, J. D. Ortiz, J. Pike, On the preservation of laminated sediments along the western margin of North America. *Paleoceanography* **18**, 1098 (2003).

94. B. K. Sen Gupta, M. L. Machain-Castillo, Benthic foraminifera in oxygen-poor habitats. *Mar. Micropaleontol.* **20**, 183–201 (1993).

95. M. Tetard, L. Licari, E. Ovsepyan, K. Tachikawa, L. Beaufort, Toward a global calibration for quantifying past oxygenation in oxygen minimum zones using benthic Foraminifera. *Biogeosciences* **18**, 2827–2841 (2021).

96. M. A. Altabet, C. Pilskaln, R. Thunell, C. Pride, D. Sigman, F. Chavez, R. Francois, The nitrogen isotope biogeochemistry of sinking particles from the margin of the Eastern North Pacific. *Deep Sea Res. Part I Oceanogr. Res. Pap.* **46**, 655–679 (1999).

97. S. E. Calvert, T. F. Pedersen, "Elemental proxies for Palaeoclimatic and Palaeoceanographic variability in marine sediments: Interpretation and application" in *Developments in Marine Geology*, vol. 1 (2007), pp. 567–644.

98. R. F. Anderson, J. P. Sachs, M. Q. Fleisher, K. A. Allen, J. Yu, A. Koutavas, S. L. Jaccard, Deep-sea oxygen depletion and ocean carbon sequestration during the last ice age. *Global Biogeochem. Cycles* **33**, 301–317 (2019).

99. Z. Lu, H. C. Jenkyns, R. E. M. Rickaby, Iodine to calcium ratios in marine carbonate as a paleo-redox proxy during oceanic anoxic events. *Geology* **38**, 1107–1110 (2010).

100. A. E. Rathburn, J. Willingham, W. Ziebis, A. M. Burkett, B. H. Corliss, A New biological proxy for deep-sea paleo-oxygen: Pores of epifaunal benthic foraminifera. *Sci. Rep.* **8**, 9456 (2018).

101. J. D. Owens, *Application of Thallium Isotopes: Tracking Marine Oxygenation through Manganese Oxide Burial* (Cambridge Univ. Press, 2019).

102. K. S. Johnson, K. H. Coale, W. M. Berelson, R. M. Gordon, On the formation of the manganese maximum in the oxygen minimum. *Geochim. Cosmochim. Acta* **60**, 1291–1299 (1996).

103. E. L. Rue, G. J. Smith, G. A. Cutter, K. W. Bruland, The response of trace element redox couples to suboxic conditions in the water column. *Deep Sea Res. Part I Oceanogr. Res.* **44**, 113–134 (1997).

104. S. J. Schenau, G. J. Reichart, G. J. de Lange, Oxygen minimum zone controlled Mn redistribution in Arabian Sea sediments during the late Quaternary. *Paleoceanography* **17**, 10–1–10–12 (2002).

105. D. Kadko, A. Aguilar-Islas, C. Bolt, C. S. Buck, J. N. Fitzsimmons, L. T. Jensen, W. M. Landing, C. M. Marsay, R. Rember, A. M. Shiller, L. M. Whitmore, R. F. Anderson, The residence times of trace elements determined in the surface Arctic Ocean during the 2015 US Arctic GEOTRACES expedition. *Mar. Chem.* **208**, 56–69 (2019).

106. J. Crusius, T. F. Pedersen, S. Kienast, L. Keigwin, L. Labeyrie, Influence of northwest pacific productivity on north Pacific intermediate water oxygen concentrations during the Bølling-Ållerød interval (14.7–12.9 ka). *Geology* **32**, 633–636 (2004).

107. I. L. Hendy, T. F. Pedersen, Oxygen minimum zone expansion in the eastern tropical North Pacific during deglaciation. *Geophys. Res. Lett.* **33**, 20 (2006).

108. B. M. Tebo, Manganese(II) oxidation in the suboxic zone of the Black Sea. *Deep Sea Res. A* **38**, S883–S905 (1991).

109. D. C. Lund, P. D. Asimow, K. A. Farley, T. O. Rooney, E. Seeley, E. W. Jackson, Z. M. Durham, Enhanced East Pacific Rise hydrothermal activity during the last two glacial terminations. *Science* **351**, 478–482 (2016).

110. J. B. Corliss, M. Lyle, J. Dymond, K. Crane, The chemistry of hydrothermal mounds near the Galapagos Rift. *Earth Planet. Sci. Lett.* **40**, 12–24 (1978).

111. J. Gottschalk, E. Michel, L. M. Thöle, A. S. Studer, A. P. Hasenfratz, N. Schmid, M. Butzin, A. Mazaud, A. Martínez-García, S. Szidat, S. L. Jaccard, Glacial heterogeneity in Southern Ocean carbon storage abated by fast South Indian deglacial carbon release. *Nat. Commun.* **11**, 6192 (2020).

112. N. Lathika, W. Rahaman, M. Tarique, N. Gandhi, A. Kumar, M. Thamban, Deep water circulation in the Arabian Sea during the last glacial cycle: Implications for paleo-redox condition, carbon sink and atmospheric CO_2 variability. *Quat. Sci. Rev.* **257**, 106853 (2021).

113. F. Lambert, M. Bigler, J. P. Steffensen, M. Hutterli, H. Fischer, Centennial mineral dust variability in high-resolution ice core data from Dome C, Antarctica, *Clim. Past* **8**, 609–623 (2012).

114. S. G. Nielsen, M. Rehkämper, D. Porcelli, P. Andersson, A. N. Halliday, P. W. Swarzenski, C. Latkoczy, D. Günther, Thallium isotope composition of the upper continental crust and rivers—An investigation of the continental sources of dissolved marine thallium. *Geochim. Cosmochim. Acta* **69**, 2007–2019 (2005).

115. M. Rehkämper, S. G. Nielsen, The mass balance of dissolved thallium in the oceans. *Mar. Chem.* **85**, 125–139 (2004).

116. S. G. Nielsen, M. Rehkämper, D. A. H. Teagle, D. A. Butterfield, J. C. Alt, A. N. Halliday, Hydrothermal fluid fluxes calculated from the isotopic mass balance of thallium in the ocean crust. *Earth Planet. Sci. Lett.* **251**, 120–133 (2006).

117. R. G. A. Baker, M. Rehkämper, T. K. Hinkley, S. G. Nielsen, J. P. Toutain, Investigation of thallium fluxes from subaerial volcanism—Implications for the present and past mass balance of thallium in the oceans. *Geochim. Cosmochim. Acta* **73**, 6340–6359 (2009).